J|A|C|S ARTICLES

Published on Web 12/18/2009

Superior Contact for Single-Molecule Conductance: Electronic Coupling of Thiolate and Isothiocyanate on Pt, Pd, and Au

Chih-Hung Ko,[†] Min-Jie Huang,[†] Ming-Dung Fu,[‡] and Chun-hsien Chen*[,†]

Department of Chemistry, National Taiwan University, Taipei, Taiwan 10617, and Department of Chemistry, National Tsing Hua University, Hsinchu, Taiwan 30013

Received October 2, 2009; E-mail: chhchen@ntu.edu.tw

Abstract: One of the critical issues for the realization of molecular electronics is the development of ideal molecule−electrode contacts that render efficient charge transportation and thus attenuate the unwanted voltage drop and power loss. The conductance at the single-molecule level has long been expected to be correlated strongly with the electrode materials. However, other than gold, systematic studies of a homologous series of molecules to extract the headgroup−metal contact conductance ($G_{n=0}$) have not been reported. Carefully examined herein are the conductances of alkanedithiols anchored onto electrode materials of Au and Pt as well as the conductances of alkanediisothiocyanates on Au, Pd, and Pt by utilizing the method of STM-BJ (scanning tunneling microscopy break junction). In comparison with Au substrate, Pd and Pt are group 10 elements with stronger d-orbital characteristics, and larger local density of states near the Fermi level. The model compounds, $SCN(CH_2)_nNCS$ ($n = 4$, 6, and 8), are studied because the isothiocyanate (-NCS) headgroup is a versatile ligand for organometallics, an emerging class of molecular wires, and can bind to substrates of noble metals to complete a metal−molecule−metal configuration for external $I-V$ measurements. Also studied include alkanedithiols, one of the most scrutinized systems in the field of single-molecule conductance. The results show that the conductance for single molecules bridged between a pair of Pt electrodes is about 3.5-fold superior to those between Au electrodes. On all electrode materials, observed are two sets of conductance values, with the smaller set being 1 order of magnitude less conductive. These findings are ascribed to the degree of electronic coupling between the headgroup and the electrode.

Introduction

Molecules exhibiting electrical properties of conducting wires,[1−10] rectification,[11,12] and negative differential resistance[13−17] have been discovered over the years, manifesting the advancement toward the realization of molecular electronics. To comprehend the electric behaviors of single molecules, quantitative measurements of their $I-V$ characteristics furnish an important constituent. Based on the primitive metal−molecule−metal (MMM) configuration, single-molecule resistance can be explored by methods of MCBJ (mechanically controllable break junction),[18−22] c-AFM (conductive atomic force microscopy),[23,24] electromigration,[25,26] STM-BJ (scanning tunneling microscopy break junction),[27−30] and STM without involving tip−substrate

[†] National Taiwan University.
[‡] National Tsing Hua University.

(1) Chen, I-W. P.; Fu, M.-D.; Tseng, W.-H.; Yu, J.-Y.; Wu, S.-H.; Ku, C.-J.; Chen, C.-h.; Peng, S.-M. *Angew. Chem., Int. Ed.* **2006**, *45*, 6244–6244.
(2) Chen, I-W. P.; Fu, M.-D.; Tseng, W.-H.; Chen, C.-h.; Chou, C.-M.; Luh, T.-Y. *Chem. Commun.* **2007**, 3074–3076.
(3) Sedghi, G.; Sawada, K.; Esdaile, L. J.; Hoffmann, M.; Anderson, H. L.; Bethell, D.; Haiss, W.; Higgins, S. J.; Nichols, R. J. *J. Am. Chem. Soc.* **2008**, *130*, 8582–8583.
(4) He, J.; Chen, F.; Li, J.; Sankey, O. F.; Terazono, Y.; Herrero, C.; Gust, D.; Moore, T. A.; Moore, A. L.; Lindsay, S. M. *J. Am. Chem. Soc.* **2005**, *127*, 1384–1385.
(5) Yin, C.; Huang, G.-C.; Kuo, C.-K.; Fu, M.-D.; Lu, H.-C.; Ke, J.-H.; Shih, K.-N.; Huang, Y.-L.; Lee, G.-H.; Yeh, C.-Y.; Chen, C.-h.; Peng, S.-M. *J. Am. Chem. Soc.* **2008**, *130*, 10090–10092.
(6) Yamada, R.; Kumazawa, H.; Noutoshi, T.; Tanaka, S.; Tada, H. *Nano Lett.* **2008**, *8*, 1237–1240.
(7) Ho Choi, S.; Kim, B.; Frisbie, C. D. *Science* **2008**, *320*, 1482–1486.
(8) Fan, F.-R. F.; Yang, J.; Cai, L.; David, W.; Price, J.; Dirk, S. M.; Kosynkin, D. V.; Yao, Y.; Rawlett, A. M.; Tour, J. M.; Bard, A. J. *J. Am. Chem. Soc.* **2002**, *124*, 5550–5560.
(9) Davis, W. B.; Svec, W. A.; Ratner, M. A.; Wasielewski, M. R. *Nature* **1998**, *396*, 60–63.
(10) Sikes, H. D.; Smalley, J. F.; Dudek, S. P.; Cook, A. R.; Newton, M. D.; Chidsey, C. E. D.; Feldberg, S. W. *Science* **2001**, *291*, 1519–1523.
(11) Metzger, R. M. *Acc. Chem. Res.* **1999**, *32*, 950–957.
(12) Böhme, T.; Simpson, C. D.; Müllen, K.; Rabe, J. P. *Chem.—Eur. J.* **2007**, *13*, 7349–7357.
(13) Chen, J.; Reed, M. A.; Rawlett, A. M.; Tour, J. M. *Science* **1999**, *286*, 1550–1552.
(14) Guisinger, N. P.; Greene, M. E.; Basu, R.; Baluch, A. S.; Hersam, M. C. *Nano Lett.* **2004**, *4*, 55–59.
(15) Xiao, X.; Nagahara, L. A.; Rawlett, A. M.; Tao, N. *J. Am. Chem. Soc.* **2005**, *127*, 9235–9240.
(16) Mentovich, E. D.; Kalifa, I.; Tsukernik, A.; Caster, A.; Rosenberg-Shraga, N.; Marom, H.; Gozin, M.; Richter, S. *Small* **2008**, *4*, 55–58.
(17) Chen, F.; He, J.; Nuckolls, C.; Roberts, T.; Klare, J. E.; Lindsay, S. *Nano Lett.* **2005**, *5*, 503–506.
(18) Reed, M. A.; Zhou, C.; Muller, C. J.; Burgin, T. P.; Tour, J. M. *Science* **1997**, *278*, 252–254.
(19) Reichert, J.; Ochs, R.; Beckmann, D.; Weber, H. B.; Mayor, M.; Löhneysen, H. v. *Phys. Rev. Lett.* **2002**, *88*, 176804.
(20) González, M. T.; Wu, S.; Huber, R.; van der Molen, S. J.; Schönenberger, C.; Calame, M. *Nano Lett.* **2006**, *6*, 2238–2242.
(21) Martin, C. A.; Ding, D.; Sørensen, J. K.; Bjørnholm, T.; van Ruitenbeek, J. M.; van der Zant, H. S. J. *J. Am. Chem. Soc.* **2008**, *130*, 13198–13199.
(22) Lötscher, E.; Ciszek, J. W.; Tour, J.; Riel, H. *Small* **2006**, *2*, 973–977.

10.1021/ja9084012

contact.[31–33] These approaches all require the molecular termini exhibiting a certain degree of affinity to the metal substrate which serves as the electrode pad being connected to an external instrumentation for control and data acquisition. The electric properties of molecular wires are described by Landauer formulation, $G = (2e^2/h)T_{lc}T_{mol}T_{rc}$, where G is the linear conductance and T_{lc}, T_{mol}, and T_{rc} respectively represent the efficiency of electron transmission through the left contact, the molecule, and the right contact.[34,35] Accordingly, it is important to develop ideal molecule−electrode contacts that exhibit efficient charge transportation and thus reduce the unwanted voltage drop and power loss. The functioning of the tailored molecule can therefore meet the expected performance.

In search of good MMM contacts, two apparent parameters that govern the conductance are the anchoring groups at the molecular termini and the electrode materials.[36,37] Several terminal groups have been studied on gold electrodes, such as thiol,[2–4,17–21,27–33,38–42] carboxylic acid (-COOH),[42] amine ($-NH_2$),[21,42–48] methyl sulfide (-SMe),[45] dimethyl phosphine ($-PMe_2$),[45] cyanide (-CN),[39] isocyanide (-NC),[39] pyridyl,[27,49,50] thiocyanate (-SCN),[6] and isothiocyanate (-NCS).[1,5,38] Generally speaking, a stronger headgroup−substrate interaction confers a larger contact conductance ($G_{n=0}$). However, the electrode materials examined thus far are predominantly gold, except two sporadic studies exploring the conductance of benzenediisocyanide and benzendithiol on platinum.[46,51] Because the conductance values are influenced by many experimental details, a systematic and thorough examination from a homologous series of molecules appears necessary to derive the intrinsic properties of the headgroup−electrode contact.

Herein, we look into the effect of electrode materials on $G_{n=0}$ by studying MMM systems of alkanethiols and alkanediisothiocyanates on Au, Pd, and Pt. The latter are group 10 elements with significant d-orbital characteristics.[36,52] The preferable binding configuration and the strength of −S and −NCS on Pd and Pt are thus expected to be different from those on the prevalently studied Au, a group 11 element exhibiting relatively stronger s-orbital contributions.[36,52] We are particularly interested in the $G_{n=0}$ of isothiocyanate because it is a versatile ligand for organometallics, an emerging class of molecular wires,[1,5,53] and because it can bind to substrates of noble metals to complete an MMM configuration for external $I-V$ characterizations. For example, SCN-M_nL_4-NCS (M_n = Cr_3, Co_3, Ni_3, Cr_5, Co_5, Ni_5, Cr_7, L = oligo-α-pyridylamido anions) are extended metal-atom chains (EMACs) in which the metal centers are collinear and wrapped helically by four equatorial ligands.[1,5] The affinity of the -NCS axial ligand toward gold electrodes makes possible the STM-BJ measurements. This electron-rich ligand extends the π conjugation and facilitates electron transporting between electrodes better than most dithiolated molecules in which, due to synthetic concerns, the termini are often coupled to thiols via a methylene linker.[2,4] For example, the decay constant β of chromium EMACs was found 0.21 $Å^{-1}$,[1,2] slightly larger than that of 0.13 $Å^{-1}$ for polyenes of benzene-furan oligoaryls.[2] However, the resistance of a single pentachromium EMAC (23.5 Å in length) is only 6.9 MΩ, ∼1/30th that of a benzene-furan oligoaryl molecule with comparable dimension (198 ± 18 MΩ, ∼22.6 Å in length).[1,2] Apparently, isothiocyanate is an effective anchoring group for organometallic wires.

α,ω-Alkanes ($SCN(CH_2)_nNCS$, n = 4, 6, 8 and $HS(CH_2)_nSH$, n = 6, 8, 10) are the model compounds in this study based on the following assessment. First, the $G_{n=0}$ values of -NCS adsorption on Pd or Pt can be obtained by a linear extrapolation of the molecular conductance to the intercept against the number of methylene units, n. Second, the saturated polymethylene chains have a large HOMO−LUMO gap which makes insignificant the development of the energy level alignment between the molecular energy level and the electrode Fermi level, E_{Fermi}. The contact conductance at the metal electrode is thus not influenced by the systematic change of n. Although the thiol headgroup is the most prevailing system for measurements of single-molecule conductance due to the rich examples of self-assembled monolayers, we found that it was very difficult to

(23) Ramachandran, G. K.; Hopson, T. J.; Rawlett, A. M.; Nagahara, L. A.; Primak, A.; Lindsay, S. M. *Science* **2003**, *300*, 1413–1416.
(24) Xu, B.; Xiao, X.; Tao, N. J. *J. Am. Chem. Soc.* **2003**, *125*, 16164–16165.
(25) Liang, W.; Shores, M. P.; Bockrath, M.; Long, J. R.; Park, H. *Nature* **2002**, *417*, 725–729.
(26) Park, J.; Pasupathy, A. N.; Goldsmith, J. I.; Chang, C.; Yaish, Y.; Petta, J. R.; Rinkoski, M.; Sethna, J. P.; Abruna, H. D.; McEuen, P. L.; Ralph, D. C. *Nature* **2002**, *417*, 722–725.
(27) Xu, B.; Tao, N. J. *Science* **2003**, *301*, 1221–1223.
(28) Ulrich, J.; Esrail, D.; Pontius, W.; Venkataraman, L.; Millar, D.; Doerrer, L. H. *J. Phys. Chem. B* **2006**, *110*, 2462–2466.
(29) Xia, J. L.; Diez-Perez, I.; Tao, N. J. *Nano Lett.* **2008**, *8*, 1960–1964.
(30) Jang, S.-Y.; Reddy, P.; Majumdar, A.; Segalman, R. A. *Nano Lett.* **2006**, *6*, 2362–2367.
(31) Haiss, W.; van Zalinge, H.; Higgins, S. J.; Bethell, D.; Hobenreich, H.; Schiffrin, D. J.; Nichols, R. J. *J. Am. Chem. Soc.* **2003**, *125*, 15294–15295.
(32) Haiss, W.; Nichols, R. J.; van Zalinge, H.; Higgins, S. J.; Bethell, D.; Schiffrin, D. J. *Phys. Chem. Chem. Phys.* **2004**, *6*, 4330–4337.
(33) Li, C.; Pobelov, I.; Wandlowski, T.; Bagrets, A.; Arnold, A.; Evers, F. *J. Am. Chem. Soc.* **2008**, *130*, 318–326.
(34) Datta, S. *Electronic Transport in Mesoscopic Systems*; Cambridge University Press: Cambridge, 2001.
(35) Salomon, A.; Cahen, D.; Lindsay, S.; Tomfohr, J.; Engelkes, V. B.; Frisbie, C. D. *Adv. Mater.* **2003**, *15*, 1881–1890.
(36) Seminario, J. M.; De La Cruz, C. E.; Derosa, P. A. *J. Am. Chem. Soc.* **2001**, *123*, 5616–5617.
(37) Yaliraki, S. N.; Kemp, M.; Ratner, M. A. *J. Am. Chem. Soc.* **1999**, *121*, 3428–3434.
(38) Fu, M.-D.; Chen, I-W. P.; Lu, H.-C.; Kuo, C.-T.; Tseng, W.-H.; Chen, C.-h. *J. Phys. Chem. C* **2007**, *111*, 11450–11455.
(39) Kiguchi, M.; Miura, S.; Hara, K.; Sawamura, M.; Murakoshi, K. *Appl. Phys. Lett.* **2006**, *89*, 213104.
(40) Li, X.; He, J.; Hihath, J.; Xu, B.; Lindsay, S. M.; Tao, N. *J. Am. Chem. Soc.* **2006**, *128*, 2135–2141.
(41) Zhou, J.; Chen, F.; Xu, B. *J. Am. Chem. Soc.* **2009**, *131*, 10439–10446.
(42) Chen, F.; Li, X.; Hihath, J.; Huang, Z.; Tao, N. *J. Am. Chem. Soc.* **2006**, *128*, 15874–15881.
(43) Venkataraman, L.; Klare, J. E.; Tam, I. W.; Nuckolls, C.; Hybertsen, M. S.; Steigerwald, M. L. *Nano Lett.* **2006**, *6*, 458–462.
(44) Venkataraman, L.; Klare, J. E.; Nuckolls, C.; Hybertsen, M. S.; Steigerwald, M. L. *Nature* **2006**, *442*, 904–907.
(45) Park, Y. S.; Whalley, A. C.; Kamenetska, M.; Steigerwald, M. L.; Hybertsen, M. S.; Nuckolls, C.; Venkataraman, L. *J. Am. Chem. Soc.* **2007**, *129*, 15768–15769.
(46) Kiguchi, M.; Miura, S.; Takahashi, T.; Hara, K.; Sawamura, M.; Murakoshi, K. *J. Phys. Chem. C* **2008**, *112*, 13349–13352.
(47) Morita, T.; Lindsay, S. *J. Phys. Chem. B* **2008**, *112*, 10563–10572.
(48) Park, Y. S.; Widawsky, J. R.; Kamenetska, M.; Steigerwald, M. L.; Hybertsen, M. S.; Nuckolls, C.; Venkataraman, L. *J. Am. Chem. Soc.* **2009**, *131*, 10820–10821.
(49) Visoly-Fisher, I.; Daie, K.; Terazono, Y.; Herrero, C.; Fungo, F.; Otero, L.; Durantini, E.; Silber, J. J.; Sereno, L.; Gust, D.; Moore, T. A.; Moore, A. L.; Lindsay, S. M. *Proc. Natl. Acad. Sci. U.S.A.* **2006**, *103*, 8686–8690.
(50) Zhou, X.-S.; Chen, Z.-B.; Liu, S.-H.; Jin, S.; Liu, L.; Zhang, H.-M.; Xie, Z.-X.; Jiang, Y.-B.; Mao, B.-W. *J. Phys. Chem. C* **2008**, xxx.
(51) Kiguchi, M.; Miura, S.; Hara, K.; Sawamura, M.; Murakoshi, K. *Appl. Phys. Lett.* **2007**, *91*, 053110.
(52) Papaconstantopoulos, D. A. In *Handbook of the Band Structure of Elemental Solids*; Plenum Press: New York, 1986; pp 157−160 and 195−202.
(53) Huang, G.-C.; Benard, M.; Rohmer, M.-M.; Li, L.-A.; Chiu, M.-J.; Yeh, C.-Y.; Lee, G.-H.; Peng, S.-M. *Eur. J. Inorg. Chem.* **2008**, *2008*, 1767–1777.

obtain well-defined conductance traces using Pd electrodes, probably due to the instability of alkanethiols on Pd substrate which catalyzes the cleavage of the C−S bond.[54,55] Therefore, parallel comparison between headgroups of isothiocyanates and thiolate is only available for Au and Pt electrodes.

The measurements of single-molecule resistance are carried out by the method of STM BJ in which the MMM junction is created by repeatedly pushing a STM tip into the surface and then retracting it away in toluene containing alkanedithiols or alkanediisothiocyanates. The STM tips of Au, Pd, or Pt fuse with the substrate during the pushing period. While pulling the tip, the merged tip−substrate joint breaks, and one or more molecules may bridge the junction.[27,28,40,42–44] In the following, we will discuss the $I-V$ characteristics of the metal−insulator−metal system, including the single-molecule resistance of alkanedithiols on Au and Pt and alkanediisothiocyanates on Au, Pd, and Pt, the tunneling decay constant, -NCS−electrode contact conductance, and the degree of electronic coupling between the headgroup and the substrate.

Experimental Section

All chemicals were reagent grade. *N*-alkanedithiols ($HS(CH_2)_nSH$, $n = 6$ from Alfa Aesar and $n = 8$, 10 from Oakwood Products) and *n*-alkanediisothiocyanates ($SCN(CH_2)_nNCS$, $n = 4$ from Alfa Aesar and $n = 6$, 8 from Oakwood Products) were used as received. Substrates were sputtered films of Au, Pd, and Pt (99.9%, Ultimate Materials Technology, Hsinchu, Taiwan) on glass slides with an adhesive underlayer of Cr (99.99%, Super Conductor Materials, Inc., Suffern, NY). Before sputtering, the glass slides were cleaned with piranha solution, a 1:3 (v/v) mixture of 30% H_2O_2 and concentrated H_2SO_4. *This solution reacts violently with organics and should be handled with great care*. The metallic films were deposited by the DC mode of a 20 W magnetron sputtering in Ar plasma (5×10^{-3} Torr) for 20 min (Co-sputtering System, Kaoduen, Taipei, Taiwan).

We followed exactly the detailed procedures and data treatment for experiments of STM break junction documented in literature reports.[27,40,42] Briefly, Au, Pd, and Pt wires with 0.1-in. diameter (99.95%, Leesan, Tainan, Taiwan) were mechanically cut by a side cutter and utilized as the STM tips. A NanoScope IIIa controller (NanoScope IIIa, Veeco, Santa Barbara, CA) was first operated in the imaging mode with the tunneling current of 1−5 nA. When the imaging showed reasonably stable images of substrates, indicative of a satisfactory tip, the instrument was switched to the mode of STS Plot $I(s)$ (scanning tunneling spectroscopy). The STM tip was brought into and out of contact with the substrate (8.4−14.0 nm/s, 1.40 Hz) in toluene (TEDIA). The subsequent tip retraction broke the tip−substrate contact and generated a molecular junction where the isothiocyanate or thiol headgroup at the termini of the polymethylene chains might bind. While acquiring current-to-tip stretching profiles, $I(s)$, the feedback loop was turned off except at the beginning point of the cycle. Regardless whether the solution contained the molecules of interest, $I(s)$ traces exhibited a stepwise profile whose steps exhibited multiples of G_o, the conductance quantum taking place when the cross section of a metallic contact is only that of a single atom ($G_o = 2e^2/h$, $\sim(12.9\ k\Omega)^{-1}$).[56−59]

The concentration of α,ω-alkanes in toluene was ∼1 mM. The stepwise $I(s)$ traces were obtained at a fixed bias voltage, and the magnitudes were orders of magnitude smaller than 1 G_o. To facilitate the determination of peak position, the preparation of the conductance histogram excluded $I(s)$ traces with simple tunneling decay which was acquired when no molecule bridged between the electrodes. It has been demonstrated by Tao et al.[42] and us[38] that incorporating all the traces in the histogram does not change the peak positions for single-molecule conductance of alkanedithiols, alkanediamines, alkanedicarboxylic acids, and alkanediisothiocyanates. The $I(s)$ traces were recorded by a NanoScope built-in program and exported as ASCII files. The data points of the stepwise traces were converted to conductance and represented a value on the histogram which indicated qualitatively how the conductance values were distributed, and only the range exhibiting peaks was shown. Gaussian function was used to fit the histograms (Origin 7.5). The peak position and standard deviation of the Gaussian curve were utilized to find the single-molecule conductance and the error bars, respectively.

To acquire single-molecule $I-V$ curves, it is necessary to obtain the values of single-molecule conductance. For example, the single-molecule conductance of $Au-S(CH_2)_6S-Au$ was 92.9 nS (vide infra), corresponding to 4.7 nA under a bias voltage of 50 mV, which were the respective settings of $i_{tunneling}$ and E_{bias} for STM imaging. After the imaging started, the instrument was switched to STS_I(V) mode, the feedback loop was turned off, and the voltage was ramping from 1.0 to −1.0 V at a scan rate of 1.4 Hz. The current as a function of the bias voltage was recorded. Most of the $I-V$ curves were simply tunneling between the electrodes. For all headgroup−electrode combinations, approximately 15% of the $I-V$ curves contained only one molecule present within the junction. The single-molecule $I-V$ curves were reconfirmed by their slopes around zero bias where single molecules appeared ohmic and the slopes laid closely to the value of single-molecule conductance.

The optimization of the geometries and calculations of the energies were carried out by using the density functional theory (DFT) method using the Gaussian 03 program, with Becke's three-parameter hybrid functional with Perdew−Wang91 correlation functional (B3PW91), the LANL2DZ relativistic effective core potential for Au, Pd, and Pt, and the 6-31+G* basis set for C, H, N, and S. Each electrode was modeled using a total of 36 atoms comprising a two-layered ($3 \times 3 \times 2$) unit cell. The lattice parameters were adapted from those of bulk materials and were fixed throughout the simulations. The calculations of Mayer 2-center bond orders were obtained using AOMix (http://www.sg-chem.net/download.php) to analyze the chemical bonding at the headgroup−electrode contact.[60,61]

The NEGF-DFT (nonequilibrium Green's function) method implemented in the ATK 2008.10 computational technique[62] was employed to calculate the transmission functions and the current−voltage characteristics for the MMM configurations. Single-ζ plus polarization (SZP) basis was used for the metals with the same electrode structures obtained from Gaussian 03. For C, H, N, and S, double-ζ plus polarization (DZP) basis set was used. Perdew−Zunger local density approximation (LDA) functional is adopted for exchange-correlation. The $I-V$ characteristics were obtained for applied biases in the range from 0.0 to 0.5 V.

Results and Discussion

$I(s)$ Traces and Conductance Histograms of Pd and Pt Atom Chains. Previous experiments on the conductance of single-atom contacts for Pd and Pt were mostly carried out under

(54) Yang, Z.; Klabunde, K. J.; Sorensen, C. M. *J. Phys. Chem. C* **2007**, *111*, 18143–18147.
(55) Ramallo-Lóez, J. M.; Giovanetti, L.; Craievich, A. F.; Vicentin, F. C.; Marín-Almazo, M.; José-Yacaman, M.; Requejo, F. G. *Phys. B* **2007**, *389*, 150–154.
(56) Olesen, L.; Laegsgaard, E.; Stensgaard, I.; Besenbacher, F.; Schiøtz, J.; Stoltze, P.; Jacobsen, K. W.; Nørskov, J. K. *Phys. Rev. Lett.* **1994**, *72*, 2251–2254.
(57) Costa-Kramer, J. L. *Phys. Rev. B* **1997**, *55*, R4875–R4878.
(58) Li, J.; Kanzaki, T.; Murakoshi, K.; Nakato, Y. *Appl. Phys. Lett.* **2002**, *81*, 123–125.
(59) Ohnishi, H.; Kondo, Y.; Takayanagi, K. *Nature* **1998**, *395*, 780–783.
(60) Gorelsky, S. I. *AOMix: Program for Molecular Orbital Analysis*; University of Ottawa: Ottawa, Ontario, Canada, 2009, http://www.sg-chem.net/.
(61) Gorelsky, S. I.; Lever, A. B. P. *J. Organomet. Chem.* **2001**, *635*, 187–196.

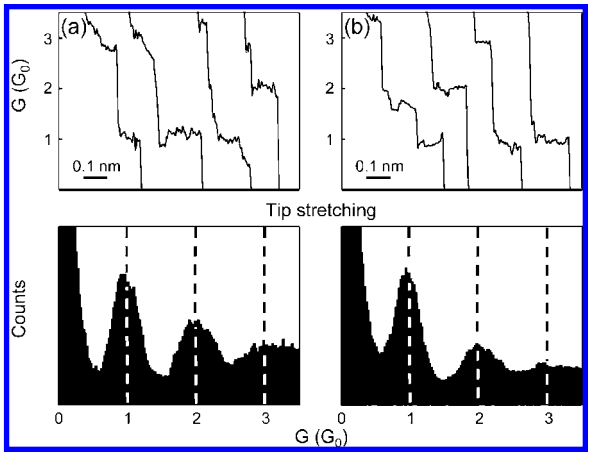

Figure 1. Results of STM BJ for (a) a Pd tip and Pd substrate and (b) a Pt tip and Pt substrate in toluene. (Upper panels) Typical current−distance traces, $I(s)$, upon stretching of the tip−substrate contact. The vertical axes represent conductance values, converted from the measured currents divided by the corresponding V_{bias} and G_o values. (Lower panels) Conductance histograms. Each histogram is prepared from more than 1000 $I(s)$ traces. The experiments carried out in air confer the same results.

vacuum. The conductance values for Pd has been controversial, including 0.5 G_o,[63] 0.9 G_o,[64,65] 1 G_o,[58] 1.6 G_o,[66] and 1.8 G_o,[67] where G_o ($= 2e^2/h \approx (12.9\ k\Omega)^{-1}$) is the conductance quantum, when the cross section of a metallic contact is that of only a single gold atom.[56–59] For Pt, reported values include 0.5 G_o,[63] 1 G_o,[56] 1.5 G_o,[68,69] and 2 G_o.[70] It is suggested that clean Pt has single-atom contacts of 1.5 G_o for zigzag configuration and 2 G_o for straight monatomic wires.[71,72] Early findings of 0.5 G_o and 1 G_o are ascribed to the presence of gas molecules which suppress the conductance of Pt.[71,72] When the measurements were performed in ambient conditions, a conductance of 1 G_o was found.[73] The results of our STM BJ measurements for Pd and Pt are displayed in Figure 1. The upper panels are typical current−distance traces, $I(s)$, taking place when the tip−substrate contact is pulled apart and the current is recorded under a couple of small bias voltages, V_{bias}. The $I(s)$ traces are presented with arbitrary x-axis offsets. The abrupt drop in current associated with the tip stretching suggests a decrease in the number of atoms at the cross section of the fused tip-substrate contact. The current values are scaled with V_{bias} and their quotient renders the conductance of metal atom chains when V_{bias} is small and the Ohm's law is obeyed. The decrease is in quantized fashion near multiples of G_o. The histograms constructed from more than one thousand $I(s)$ traces show peaks near 1 G_o and 2 G_o, corresponding to the conductance of the metal wires with diameters of 1 and 2 atoms and thus exhibiting the fundamental conductance of 1.0 ± 0.2 G_o for both Pd and Pt. The results are indistinguishable for measurements carried out in air and in toluene.

***I*(*s*) Traces and Conductance Histograms for α,ω-Alkanes.** The $I(s)$ traces and histograms shown in Figure 2 are the results for $HS(CH_2)_nSH$ and $SCN(CH_2)_nNCS$. Panels a−c and g−i were via Pt contacts, and panels d−f were obtained by using Pd tips and Pd substrates. Around the corresponding current range, controlled experiments in blank solution (toluene) result in exponential traces of tunneling decay, confirming that the staircase waveforms and peaks in the histograms arise from the α,ω-alkanes. Table 1 summarizes single-molecule conductance measured at the junctions of Pd and Pt electrodes. For better comparison, the results from our previous study[38] on Au electrodes are also incorporated. The conductance values of alkanedithiols on Pt and alkanediisothiocyanates on Pd and on Pt are about 1.5−3.5-fold superior to those on Au, demonstrating the significant influence of the electrode materials on the measured conductance.

With careful examination, another set of peaks with the feature of integer multiples can be found. The results are displayed in the insets. The two sets are termed HC and LC abbreviated for high and low conductance values, respectively. Two sets of conductance histograms have been observed in the cases of thiol[38,42] and isothiocyanate[38] headgroups on gold. It is a general consensus that the headgroup-substrate binding geometry plays a significant role in the conductance values which are larger for those with the headgroup on 3-fold hollow sites and smaller for those residing on atop sites.[40] During the measurements, HC and LC traces are acquired when the molecular termini are sitting, respectively, on atop and hollow sites of the gold substrate (denoted as atop−hollow) and on two atop sites (atop−atop). The case of hollow−hollow configuration is excluded because the MMM junctions are developed by pulling the metal atoms out of the electrodes and resulting in at least an atop geometry at the junctions. Tao, Lindsay and co-workers presented a thorough study on this matter.[40] For headgroups lack of preferential adsorption sites, e.g. -NH_2 on gold, both one[43–45] and two sets[40] of conductance values have been reported.

The ratios of HC to LC for are about 6 folds on Au and Pt of alkanedithiols. For alkanediisothiocyanates on Pd and Pt, the ratios of HC to LC are about 12 folds, quite similar to the 10-fold ratio found on gold electrodes.[38] The probability for $I(s)$ traces exhibiting MMM characteristics for hexanedithiol on Pt is 30%, similar to that of 35% on Au. For butanediisothiocyanate, the frequency to collect the stepwise traces is about 37% for Pd and 42% for Pt, significantly larger than the ~27% found for the same molecule on Au.[38] The discrepancy is attributed to stronger adsorption of isothiocyanate on Pd and Pt than that on Au (vide infra).

Insulating Properties of α,ω-Alkanes. One of the reasons to employ α,ω-alkanes as the model system is that the contact conductance of the -NCS-electrode and -S-electrode can be greatly simplified by taking advantage of the large HOMO−LUMO gap of methylene chains. To valid this assumption, Simmons' model[74] that describes insulating barrier parameters

(62) *ATK (Atomistix ToolKit)*, version 2008.2010; QuantumWise: Copenhagen, Denmark, http://www.atomistix.com/
(63) Rodrigues, V.; Bettini, J.; Silva, P. C.; Ugarte, D. *Phys. Rev. Lett.* **2003**, *91*, 096801.
(64) Kiguchi, M.; Murakoshi, K. *Appl. Phys. Lett.* **2006**, *88*, 253112.
(65) Zhou, X.-S.; Wei, Y.-M.; Liu, L.; Chen, Z.-B.; Tang, J.; Mao, B.-W. *J. Am. Chem. Soc.* **2008**, *130*, 13228–13230.
(66) Tomoko, M.; Tokushi, K. *Jpn. J. Appl. Phys.* **2007**, *46*, 4370–4374.
(67) Csonka, S.; Halbritter, A.; Mihály, G.; Shklyarevskii, O. I.; Speller, S.; van Kempen, H. *Phys. Rev. Lett.* **2004**, *93*, 016802.
(68) Sirvent, C.; Rodrigo, J. G.; Vieira, S.; Jurczyszyn, L.; Mingo, N.; Flores, F. *Phys. Rev. B* **1996**, *53*, 16086–16090.
(69) Kiguchi, M.; Tal, O.; Wohlthat, S.; Pauly, F.; Krieger, M.; Djukic, D.; Cuevas, J. C.; van Ruitenbeek, J. M. *Phys. Rev. Lett.* **2008**, *101*, 046801.
(70) Smit, R. H. M.; Untiedt, C.; Yanson, A. I.; van Ruitenbeek, J. M. *Phys. Rev. Lett.* **2001**, *87*, 266102.
(71) Pauly, F.; Dreher, M.; Viljas, J. K.; Häfner, M.; Cuevas, J. C.; Nielaba, P. *Phys. Rev. B* **2006**, *74*, 235106.
(72) Smogunov, A.; Corso, A. D.; Tosatti, E. *Phys. Rev. B* **2008**, *78*, 014423.
(73) Costa-Krämer, J. L. *Phys. Rev. B* **1997**, *55*, R4875–R4878.
(74) Simmons, J. G. *J. Appl. Phys.* **1963**, *34*, 1793–1803.

in metal−insulator−metal junctions is employed to simulate the single-molecule $I-V$ curves of hexanedithiol and butanediisothiocyanate, the shortest molecule in this homologous series and thus the most conductive ones:

$$I \propto e\left(\phi_B - \frac{V_{bias}}{2}\right)\exp\left[-\frac{2(2m)^{1/2}e^{1/2}}{\hbar}\alpha\left(\phi_B - \frac{V_{bias}}{2}\right)^{1/2}L\right] - e\left(\phi_B - \frac{V_{bias}}{2}\right)\exp\left[-\frac{2(2m)^{1/2}e^{1/2}}{\hbar}\alpha\left(\phi_B - \frac{V_{bias}}{2}\right)^{1/2}L\right]$$

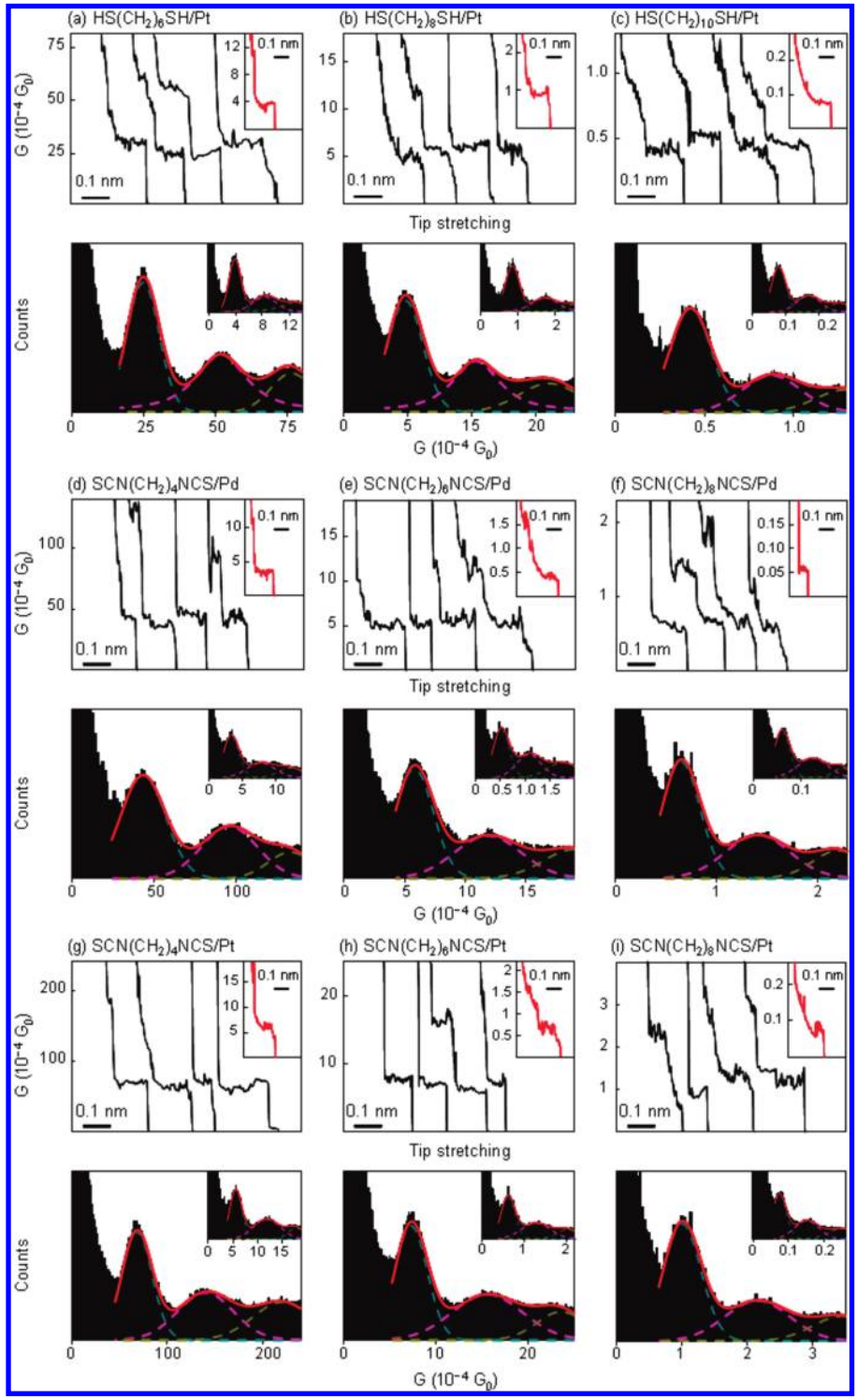

Figure 2. Single-molecule conductance measurements by STM BJ studies on Pt for $HS(CH_2)_nSH$ with n = (a) 6, (b) 8, and (c) 10. $SCN(CH_2)_nNCS$ with n = 4 (d, g), 6 (e, h), and 8 (f, i) are measured on (d−f) Pd and on (g−i) Pt. (Upper panels) Typical $I(s)$ traces acquired upon stretching of the molecular junctions. (Lower panels) Conductance histograms plotted from more than 1500 $I(s)$ traces. The experiments were carried out in toluene. (Inset) Histograms for low-conductance sets where the conductance values are about 1/12 those of the high-conductance ones. Peak positions were determined using Gaussian fits to the profiles of histograms. The red lines are the sums of the Gaussians. The standard deviations estimated from the Gaussian fittings were used as the error bars in the subsequent figures. In the absence of alkanediisothiocyanates, no conductance steps were observed from $I(s)$ traces, and no peaks were found in the histograms within the same conductance range.

Table 1. Summary of Single-Molecule Conductance for Alkanedithiols and Alkanediisothiocyanates on Au, Pd, and Pt Electrodes

	Au-S-$(CH_2)_n$-S-Au junctions[38]		Pt-S-$(CH_2)_n$-S-Pt junctions		Au-SCN-$(CH_2)_n$-NCS-Au junctions[38]		Pd-SCN-$(CH_2)_n$-NCS-Pd junctions		Pt-SCN-$(CH_2)_n$-NCS-Pt junctions	
n	HC[a]	LC[a]	HC	LC	HC	LC	HC	LC	HC	LC
	G ($\times 10^{-4}$ G_o)[b]	G ($\times 10^{-4}$ G_o)	G ($\times 10^{-4}$ G_o)	G ($\times 10^{-4}$ G_o)	G ($\times 10^{-4}$ G_o)	G ($\times 10^{-4}$ G_o)	G ($\times 10^{-4}$ G_o)	G ($\times 10^{-4}$ G_o)	G ($\times 10^{-4}$ G_o)	G ($\times 10^{-4}$ G_o)
4	–	–	–	–	19 ± 4	2.0 ± 0.4	43 ± 13	3.4 ± 1.1	69 ± 15	5.7 ± 1.2
6	12 ± 2	2.2 ± 0.4	25 ± 6	3.9 ± 0.9	2.0 ± 0.4	0.20 ± 0.04	5.9 ± 1.5	0.51 ± 0.16	7.3 ± 1.7	0.64 ± 0.16
8	2.6 ± 0.4	0.59 ± 0.06	4.8 ± 1.4	0.85 ± 0.19	0.34 ± 0.07	0.043 ± 0.009	0.66 ± 0.21	0.060 ± 0.016	1.0 ± 0.3	0.075 ± 0.019
10	0.22 ± 0.04	0.043 ± 0.009	0.42 ± 0.11	0.078 ± 0.021	–	–	–	–	–	–

[a] HC and LC denote high- and low-conductance data sets, respectively. [b] The values of G are interconvertible through $G_o = (12.9\ k\Omega)^{-1}$. The standard deviations were obtained from Gaussian fitting.

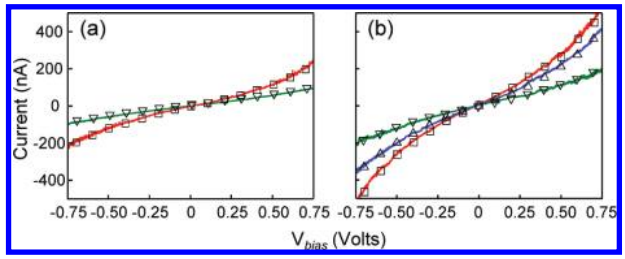

Figure 3. Single molecule $I-V$ characteristics of the HC set of (a) hexanedithiol and (b) butanediisothiocyanate. The green, blue, and red curves are the experimental single-molecule $I-V$ curves acquired using Au, Pd, and Pt electrodes, respectively. The $I-V$ curves for hexanedithiol on Pd are not acquired probably due to a breakage of C–S bond on Pd.[54] The superimposed symbols are simulated results for the corresponding curves by Simmons' formula.

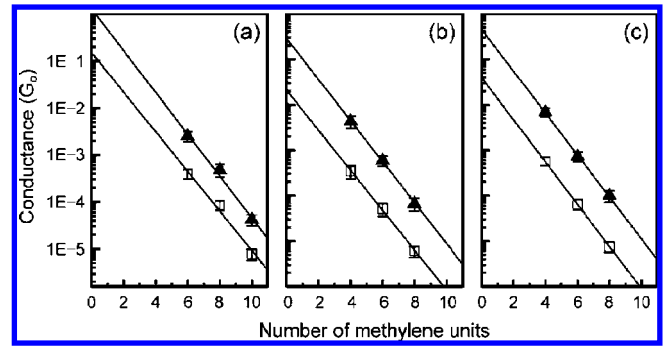

Figure 4. Semilogarithmic plots of single-molecule conductance versus number of methylene units for MMM junctions of (a) Pt-S-$(CH_2)_n$-S-Pt, (b) Pd-SCN-$(CH_2)_n$-NCS-Pd, and (c) Pt-SCN-$(CH_2)_n$-NCS-Pt. Symbols: solid triangles, HC; open squares, LC: The slopes and y intercepts of the best-fit lines yield the tunneling decay factor, β_n, and the contact conductance, $G_{n=0}$, respectively.

Derived from the Wentzel–Kramer–Brillouin approximation,[75,76] this formulation describes that under an intermediate-voltage range of bias (V_{bias}, in volts) the current (I, in amperes) is a result of electron tunneling across a rectangular barrier height ϕ_B (in volts) between electrodes spaced by a thin insulating film with a thickness of L (in meters). m, e, and η are respectively the rest mass of an electron (in kg), the charge of an electron (in coulombs), and Planck's constant divided by 2π (in J·s). To make the formulation generalized for any shape of potential barrier, Simmons introduced α which, by itself, does not provide physical meanings about the structure of the barrier.[74,77,78] Simmons formula shows that at a very small V_{bias} the current is dependent on the barrier width L as $i = (V_{bias}/R)e^{-\beta L}$ where β (in $Å^{-1}$) is a bias-independent decay constant.

$$\beta = \frac{2(2m)^{1/2}e^{1/2}}{\hbar}\alpha\phi_B^{1/2} \approx 1.03\alpha\phi_B^{1/2}$$

Similarly, for molecules having a larger n (i.e., a longer methylene chain), the conducting current decreases exponentially, expressed by $i = (V_{bias}/R)e^{-\beta_n n}$.

Figure 3 displays the single-molecule $I-V$ curves of hexanedithiols on Au and Pt electrodes and butanediisothiocyanates on Au, Pd, and Pt electrodes. The experimental procedures to acquire $I-V$ curves from which the MMM junction has only one single molecule are described in the Experimental Section.[27,40,42] The current values at the linear $I-V$ regime agree with those of the HC fundamental peaks in the $I(s)$ histograms (Figure 2). The Simmons' model is then utilized to fit the $I-V$ characteristics of Figure 3. By employing L of 0.94 and 1.12 nm estimated from MM2 calculations (Chem3D), respectively, for hexanedithiol and butanediisothiocyanate, the best fitting results for the HC sets are tabulated in Table 2. The resulting parameters, ϕ_B, α, and β are indistinguishable despite their current values are strongly associated with the electrode materials. Explicitly, the almost identical values of ϕ_B suggest that the molecule within the electrodes can thus be thought of as a tunnel barrier, supporting our choice of α,ω-alkane moiety that bears a large HOMO–LUMO gap. Therefore, the difference in their conductance has to be ascribed to the contact with the electrode materials.

Contact Conductance and $I-V$ Characteristics of α,ω-Alkanes. Figure 4 shows how β_n and $G_{n=0}$ are derived by plotting the resistance values from Table 1 against the number of methylene units of the molecules. The tunneling decay constants, β_n and β, for a homologous series are extracted from $G \propto \exp(\beta_n n)$ and $\exp(\beta L)$, where n and L are respectively the number of methylene units and the molecular length (in Å). The straight lines fitted in Figure 4 describe the exponential increase in the single-molecule resistance as a function of the molecular chain length, suggesting a coherent and nonresonant tunneling. The slopes of the least-squares lines give the β_n values

Table 2. Fitting Summary of Tunneling Barrier Height (ϕ_B) and Decay Constant (β) via Simmons Formula

electrode material (M)	M-S-$(CH_2)_6$-S-M junctions			M-SCN-$(CH_2)_4$-NCS-M junctions		
	barrier height, ϕ_B (eV)	α[a]	$\beta = \alpha \times \phi_B^{1/2}$ ($Å^{-1}$)	barrier height, ϕ_B (eV)	α	$\beta = \alpha \times \phi_B^{1/2}$ ($Å^{-1}$)
Au	1.34 ± 0.04	0.70 ± 0.01	0.81 ± 0.02	1.30 ± 0.05	0.66 ± 0.02	0.75 ± 0.03
Pd	–[b]	–[b]	–[b]	1.36 ± 0.13	0.68 ± 0.04	0.79 ± 0.06
Pt	1.42 ± 0.27	0.73 ± 0.08	0.87 ± 0.14	1.32 ± 0.17	0.70 ± 0.05	0.83 ± 0.06

[a] α is a fitting parameter and does not provide physical meaning by itself (see text).[74] [b] $I-V$ curves was unavailable for hexanedithiol on Pd substrate (see text for details).[54]

of ~1.0 per CH_2 for both HC and LC sets of alkanedithiols and alkanediisothiocyanates (see Table 3). The β_n values are practically the same as those reported values for alkane with various headgroups. Therefore, the discrepancy in their single-molecule resistance should arise from the electrode materials.

In Figure 4 the extrapolation of the least-squares fitting to the intercept renders the respective HC (triangles) and LC (squares) contact conductance, $G_{n=0}$. The values of $G_{n=0}$ for -S-Pt is about twice that of -S-Au (Table 3). The values of $G_{n=0}$ for -NCS-Pd and -NCS-Pt electrodes are about 3−5-fold more conductive than those of -NCS-Au (Table 3). This result of the π-conjugated headgroup is significant in that the contact composed of two -NCS-Pt has four bonds longer than that of dithiols on Au yet the values of $G_{n=0}$ are close.

Transmission Spectra. It is intriguing that the $G_{n=0}$ of molecules on Pt is significantly superior to those on Au. Similar discrepancies found for different headgroups on gold have been widely explained by the energy level alignment between the molecular electronic levels and the electrode E_{Fermi}.[42,45,79–86] Displayed in Figure 5 are transmission spectra at zero bias for molecules containing six methylene units. The solid and dashed traces represent the transmission versus energy shift from E_{Fermi} for molecules bridging, respectively, in the atop−hollow (HC) and atop−atop (LC) configurations. The HOMO−LUMO gaps are in a good agreement with literature reports of 7−9 eV for α,ω-alkanes.[87–89] By integrating the transmission with bias voltages ranging from 0 to 0.5 V, we obtain simulated $I-V$ curves (not shown) from which the slopes at the ohmic region (~0−0.2 V) yield single-molecule conductance reported in Table 4. The trend in which Pt shows the largest conductance and Au the smallest is consistent with the experimental results. However, this finding is not apparent from Figure 5 because the spectra are featureless around E_{Fermi} and because the large HOMO−LUMO gaps make negligibly small the variation of the tunneling barrier height that arises from the difference between the E_{Fermi} of Au, Pd, and Pt.[90] In addition, Au and Pd have almost identical work function and thus have similar E_{Fermi}, yet they furnish considerably different conductance for alkanediisothiocyanates. Apparently, the model of energy level alignment does not explain well the difference in the single-molecule conductance on these electrodes. Thus, we look into the electronic coupling at the headgroup−electrode contact.

Binding Geometries and Electronic Coupling between Headgroup and Electrode. To provide details on the contact and on the origin of the multiple conductance data sets, the occurrences for HC-only or LC-only events over the total number of stepwise traces are counted and summarized in the last row of Table 3.

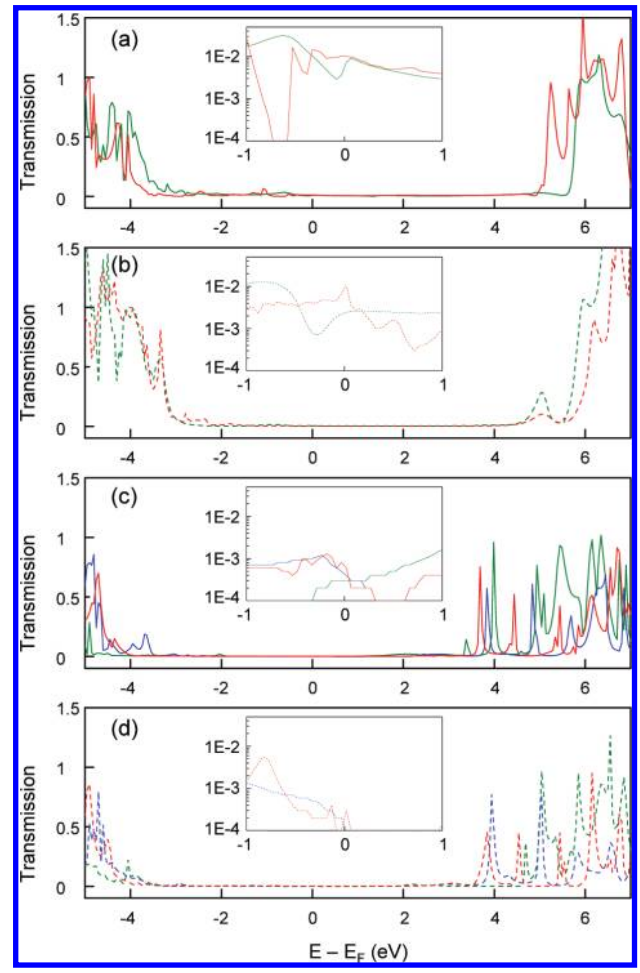

Figure 5. Zero-bias transmission versus energy shifted from the Fermi energy. MMM configurations: (a) M-S-$(CH_2)_6$-S-M, atop−hollow; (b) M-S-$(CH_2)_6$-S-M, atop−atop; (c) M-SCN-$(CH_2)_6$-NCS-M, atop−hollow; (d) M-SCN-$(CH_2)_6$-NCS-M, atop−atop. M = Au (green), Pd (blue), Pt (red). (Inset) Semilogarithmic plot within ±1 V.

The probability for $I(s)$ traces exhibiting both HC and LC behaviors is presented in the table footnote. For the cases involving thiolate-Pt contacts, HC traces are acquired more often than the LC ones, the same as those of dithiols on Au. For the isothiocyanate headgroup, the frequency of HC traces taking place on Pd or Pt contacts is also higher than that of LC traces, interestingly, opposite to that on Au. Such disparity in probability prompts us to scrutinize the headgroup−electrode binding geometries by DFT calculations.

Table 3. Summary of β_n, $G_{n=0}$, and Frequency of Observation of HC and LC Data Sets[a] for α,ω-Alkanes on Au, Pd, and Pt Electrodes

	Au-S-$(CH_2)_n$-S-Au junctions[38]		Pt-S-$(CH_2)_n$-S-Pt junctions		Au-SCN-$(CH_2)_n$-NCS-Au junctions[38]		Pd-SCN-$(CH_2)_n$-NCS-Pd junctions		Pt-SCN-$(CH_2)_n$-NCS-Pt junctions	
	HC[a]	LC[a]	HC	LC	HC	LC	HC	LC	HC	LC
β_n (per CH_2)	1.01 ± 0.14	0.98 ± 0.19	1.00 ± 0.19	1.05 ± 0.11	1.01 ± 0.07	0.96 ± 0.07	1.04 ± 0.13	1.01 ± 0.12	1.07 ± 0.10	1.08 ± 0.11
β (per Å)[b]	0.79 ± 0.11	0.77 ± 0.15	0.80 ± 0.07	0.84 ± 0.09	0.80 ± 0.06	0.75 ± 0.05	0.83 ± 0.10	0.81 ± 0.10	0.86 ± 0.08	0.86 ± 0.09
$G_{n=0}$ (G_o)[c]	0.60 ± 0.70	0.10 ± 0.15	1.08 ± 0.81	0.33 ± 0.28	0.10 ± 0.05	0.008 ± 0.004	0.29 ± 0.23	0.020 ± 0.015	0.48 ± 0.28	0.042 ± 0.026
$R_{n=0}$ (kΩ)[c]	22 ± 25	130 ± 200	12 ± 9	39 ± 33	128 ± 59	1560 ± 720	45 ± 36	646 ± 501	27 ± 16	307 ± 188
probability (%)[d]	51	33	57	32	34	58	47	40	55	34

[a] HC and LC denote high- and low-conductance data sets, respectively. [b] β is estimated by employing L of 0.94, 1.19, and 14.4 nm for hexyl, octyl, and decanedithiolate, respectively. L of butyl, hexyl, and octanediisothiocyanates is 1.12, 1.37, and 1.62 nm, respectively. The calculations are based on MM2 calculations (molecular mechanics calculator 2, embedded in Chem3D). [c] $G_{n=0}$ and $R_{n=0}$ are, respectively, the contact conductance and contact resistance obtained from the intercepts of Figure 4. [d] The values of probability in the table do not include traces that exhibit both HC and LC steps. The percentages of traces that show both HC and LC currents are ~8%, 13%, and 12% for SCN-$(CH_2)_4$-NCS on Au, Pd, Pt, and ~12% and 11% for HS-$(CH_2)_6$-SH on Au and Pt, respectively. Frequency of occurrence is reported only for SCN-$(CH_2)_4$-NCS and HS-$(CH_2)_6$-SH because of their larger current values, better-defined $I(s)$ traces, and thus more conclusive results than obtained for the other molecules.

Table 4. Calculated Single-Molecule Conductance of α,ω-Alkanes on Atop−Hollow (HC) and Atop−Atop (LC) Configurations of Au, Pd, and Pt

	Au-S-$(CH_2)_n$-S-Au junctions		Pt-S-$(CH_2)_n$-S-Pt junctions		Au-SCN-$(CH_2)_n$-NCS-Au junctions		Pd-SCN-$(CH_2)_n$-NCS-Pd junctions		Pt-SCN-$(CH_2)_n$-NCS-Pt junctions	
	HC[a]	LC[a]	HC	LC	HC	LC	HC	LC	HC	LC
n	G ($\times 10^{-4}$ G_o)	G ($\times 10^{-4}$ G_o)	G ($\times 10^{-4}$ G_o)	G ($\times 10^{-4}$ G_o)	G ($\times 10^{-4}$ G_o)	G ($\times 10^{-4}$ G_o)	G ($\times 10^{-4}$ G_o)	G ($\times 10^{-4}$ G_o)	G ($\times 10^{-4}$ G_o)	G ($\times 10^{-4}$ G_o)
4	–	–	–	–	9.16	2.67	16.3	6.32	23.8	8.05
6	62.1	18.0	89.9	44.0	3.09	0.833	4.06	1.18	5.11	1.58
8	13.8	1.97	21.4	8.49	0.314	0.0938	0.616	0.205	0.769	0.237
10	2.01	0.300	2.48	1.51	–	–	–	–	–	–

[a] HC and LC denote high- and low-conductance data sets, respectively.

Table 5. DFT Calculations of Adsorption of Mercaptohexane and Isothiocyanatobutane on Au, Pd, and Pt Electrodes

	$CH_3(CH_2)_5$-S-M				$CH_3(CH_2)_3$-NCS-M			
	adsorption energy (eV)				adsorption energy (eV)			
electrode material (M)	three-fold hollow site	atop site	angle (∠CSM) (deg)	σ:π characteristics (S−M) (%)[b]	three-fold hollow site	atop site	angle (∠CSM) (deg)	σ:π characteristics (S−M) (%)[b]
Au	−1.651	−1.211	104.22	99.5:0.5	−0.816	−1.125	103.19	96.8:3.2
Pd	–[a]	–[a]	–[a]	–[a]	−1.421	−1.289	178.10	76.7:23.3
Pt	−1.735	−1.362	108.44	89.6:10.4	−1.623	−1.338	179.43	68.0:32.0

[a] Calculations were not carried out due to the catalytic reaction of breaking S−C bond for thiolates on Pd substrate (see text).[54] [b] Calculations carried out by AOMix program.

The molecules simulated for revealing binding configurations and the corresponding adsorption energy are mercaptohexane and isothiocyanatobutane, instead of the more complicated α,ω-alkanes, to make simpler the study of headgroup−substrate interactions. The molecular structures are optimized prior to the calculations and are fixed in the subsequent simulations. The DFT modeling summarized in Table 5 shows that, except for isothiocyanatohexane on gold, the adsorption on the 3-fold hollow site is a few tenths of an eV more stable than that on the atop site. The trend agrees with the occurrence of HC and LC data sets for all cases, consistent with the aforementioned consensus that the HC and LC traces are attributed to the binding schemes of the atop−hollow and the atop−atop configurations,

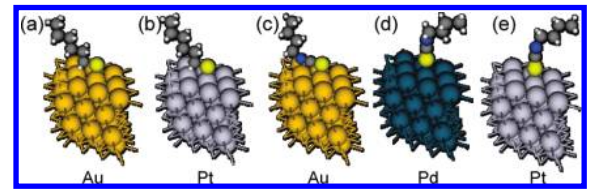

Figure 6. Side views of mercaptohexane adsorbed on atop sites of (a) Au and (b) Pt and isothiocyanatobutane on (c) Au, (d) Pd, and (e) Pt. Details of DFT calculations and the degrees of ∠MSC are referred to in the Experimental Section and Table 5, respectively.

respectively. Therefore, larger adsorption energy preferably renders a higher frequency for the corresponding data set.

Figure 6 shows the results that the angles of both ∠CSAu and ∠CSPt for mercaptohexane are about 104°. In the case of isothiocyanate, ∠CSAu has a bent angle of 103°, yet ∠CSPd and ∠CSPt appear linear. The angles of ∼104° and 180° imply a significant contribution from σ and π components. A quantitative measure is accessed using Mayer 2-center bond-order calculations to gain additional insight. The sulfur−metal bond orders of -S-Au, -S-Pt, -NCS-Au, -NCS-Pd, and -NCS-Pt are found to be respectively 0.837, 1.280, 0.393, 0.660, and 0.739 which show a good correlation with the measured contact conductance (Figure 7). Further analysis of the headgroup−metal bond orders reveals that the relative contributions of π to σ characters for the cases of -NCS-Pd, and -NCS-Pt are respectively 1/3 and 1/2 (Table 5). Even for -S-Pt that has a ∠CSPt angle of 108°, the π contribution does not appear negligible. Literature reports[36,52] show that the s-orbital contribution on Au is roughly 3 times stronger than those on group 10 elements of Pd and Pt, suggesting that σ bonding is preferably adopted on Au surface even for adsorbate with a relatively strong π character such as -NCS. Pd and Pt have significant d-orbital contribution and thus exhibit a linear bonding scheme with -NCS. Alternatively, the relative magnitude of $G_{n=0}$ for headgroup−electrode contacts can be rationalized qualitatively by the extent of π character mixing into the binding.[36,45] The presence of π character at the contact implies an additional channel available for electron transfer and thus more conductive than those with σ

(75) Messiah, A. Classical Approximation and the WKB Method. In *Quantum Mechanics*; North-Holland Publishers: Amsterdam, 1964; pp 214−242.
(76) Davydov, A. S. *The Connection between Quantum Mechanics and Classical Mechanics*, 2nd ed.; Pergamon Press: Oxford: U.K., 1976; pp 71−86.
(77) Holmlin, R. E.; Haag, R.; Chabinyc, M. L.; Ismagilov, R. F.; Cohen, A. E.; Terfort, A.; Rampi, M. A.; Whitesides, G. M. *J. Am. Chem. Soc.* **2001**, *123*, 5075–5085.
(78) Wang, W.; Lee, T.; Reed, M. A. *Phys. Rev. B* **2003**, *68*, 035416.
(79) Venkataraman, L.; Park, Y. S.; Whalley, A. C.; Nuckolls, C.; Hybertsen, M. S.; Steigerwald, M. L. *Nano Lett.* **2007**, *7*, 502–506.
(80) Engelkes, V. B.; Beebe, J. M.; Frisbie, C. D. *J. Am. Chem. Soc.* **2004**, *126*, 14287–14296.
(81) Kim; Beebe, J. M.; Jun, Y.; Zhu, X. Y.; Frisbie, C. D. *J. Am. Chem. Soc.* **2006**, *128*, 4970–4971.
(82) Xue, Y.; Datta, S.; Ratner, M. A. *J. Chem. Phys.* **2001**, *115*, 4292–4299.
(83) Heimel, G.; Romaner, L.; Brédas, J.-L.; Zojer, E. *Phys. Rev. Lett.* **2006**, *96*, 196806.
(84) Beebe, J. M.; Kim, B.; Frisbie, C. D.; Kushmerick, J. G. *ACS Nano* **2008**, *2*, 827–832.
(85) Li, X. L.; Hihath, J.; Chen, F.; Masuda, T.; Zang, L.; Tao, N. J. *J. Am. Chem. Soc.* **2007**, *129*, 11535–11542.
(86) Cohen, R.; Stokbro, K.; Martin, J. M. L.; Ratner, M. A. *J. Phys. Chem. C* **2007**, *111*, 14893–14902.
(87) Less, K. J.; Wilson, E. G. *J. Chem. Phys.* **1973**, *6*, 3110–3121.
(88) Wu, S.; Gonzalez, M. T.; Huber, R.; Grunder, S.; Mayor, M.; Schonenberger, C.; Calame, M. *Nat. Nanotechnol.* **2008**, *3*, 569–574.
(89) Boulas, C.; Davidovits, J. V.; Rondelez, F.; Vuillaume, D. *Phys. Rev. Lett.* **1996**, *76*, 4797.
(90) Michaelson, H. B. *J. Appl. Phys.* **1977**, *48*, 4729–4733.

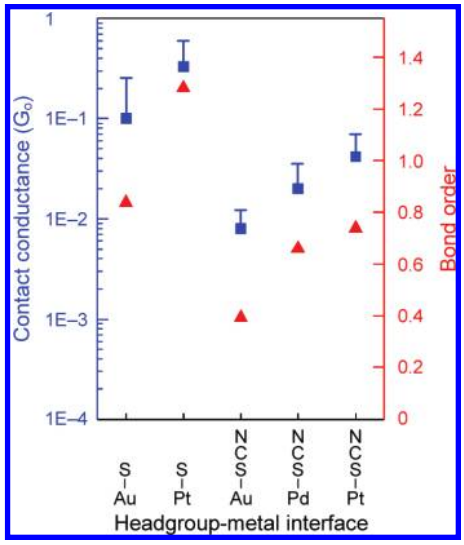

Figure 7. Correlation between $G_{n=0}$ and Mayer bond order at molecule−electrode contact. Blue squares (left scale): measured $G_{n=0}$; red triangle (right scale): bond order.

character alone. Therefore, the superior conductance of α,ω-alkanes on Pd and Pt is ascribed to their π characters.

Conclusions

This study demonstrates the importance of the electronic coupling at the headgroup−electrode contact on the measured single-molecule conductance. To focus on the properties of the electrode materials, α,ω-alkanes are the model compounds because their large HOMO−LUMO gaps make insignificant the effect of the energy alignment at the molecule−electrode interface. This assumption is supported by the simulated transmission spectra and by fitting using Simmons' formula which reveals similar barrier heights, ∼1.3 eV, for all α,ω-alkanes examined. Pt electrodes offer the single-molecule conductance of alkanedithiols and alkanediisothiocyanates, respectively, about 2−3.5-fold superior to those on Au. The contact conductance, $G_{n=0}$, for thiolate-Pt is twice that of thiolate-Au and for isothiocyanate-Pt, a π-rich ligand, is found to be 5-fold superior to that of Au. The calculated bond angles of ∠MSC and the analysis of Mayer bond order suggest that at Pt and Pd contacts π characters are significantly involved, while at Au contacts it is predominantly σ characters. Therefore, the electronic coupling plays an important factor on $G_{n=0}$ and on the measured single-molecule conductance.

Acknowledgment. This work was supported by Center for Advanced Nano-Materials, College of Science (NTU, 95R0034-02), National Science Council of ROC through Grants NSC-95-2113-M-002-036 and NSC-95-2752-M-002-001-PAE. We acknowledge the National Center for High-Performance Computing of Taiwan for generous amounts of computing time.

JA9084012